Acta Otolaryngol (Stockh) 1989; Suppl. 467: 241–248

CHAPTER 29

Models of Nonlinear Vibration. I. Oscillator with Bilinear Resistance

SUZANNE E. KEILSON,[1] MALVIN C. TEICH[1] and SHYAM M. KHANNA[2]

Columbia University, Departments of [1]Applied Physics and [2]Otolaryngology, New York, USA

INTRODUCTION

The forced linear harmonic oscillator has three constant elements—mass, resistance, and stiffness—in addition to a forcing function. The simplest one-dimensional oscillators that exhibit tuning and are inherently nonlinear are the bilinear oscillators. In these oscillators, the magnitude of one of these elements depends on the oscillator displacement, assuming one of two possible values depending on the sign of the displacement with respect to an arbitrary origin. The other two elements remain constant, independent of displacement. All of these oscillators exhibit complex dynamical behavior. The bilinear stiffness and bilinear mass oscillators are considered in companion papers (Teich, Keilson and Khanna, 1989; Keilson, Teich and Khanna, 1989). The bilinear resistance (bilinear damping) oscillator considered here exhibits a resistance with value r_1 when the displacement is positive with respect to an arbitrary origin and a resistance r_2 when it is negative with respect to that origin.

THEORY

The equation of motion of a bilinear resistance oscillator is

$$mx''(t)+r(x)\,x'(t)+kx(t) = A_o \cos(2\pi f_s t), \tag{1}$$

where x, x′, and x″ represent displacement, velocity, and acceleration, respectively. This is an ordinary, nonlinear, nonautonomous differential equation since the resistance coefficient r(x) is a function of the displacement x and the time t appears as an explicit variable in the forcing function. The forcing function has an amplitude A_o and a frequency f_s. For the bilinear resistance oscillator,

$$r(x) = r_1 \quad \text{for } x \geq 0$$
$$r(x) = r_2 \quad \text{for } x < 0. \tag{2}$$

We generated computer solutions to this equation by using a fourth-order Runge-Kutta algorithm (Scraton, 1984; Press et al., 1986), which provides a numerical method for iterating through discrete time steps to determine the displacement as a function of time. Our calculations were carried out on a Compaq Model 386 desktop personal computer. As a result of the form of Eq. (2), the solution scales linearly with the amplitude of the forcing function A_o so that the normalized displacement and velocity, and their spectra, do not change with the applied signal level. For the case of arbitrary r(x), the solution does not in general scale linearly with A_o so that the results will depend on the amplitude of the forcing function. A smoother set of solutions is obtained if the resistance coefficient is a bilinear function of the velocity x′ rather than the displacement x.

The numerical solution to the differential equation was usually calculated with an iteration step size of 40 microseconds and an array vector of 1024 bins, giving a total time course of 0.041 seconds for the calculated waveform. With this sampling step size, the Nyquist frequency is 12.5 kHz and the frequency resolution of the discrete Fourier transform (DFT) is 24.41 Hz. These numbers were chosen to accord with the values used in experimental data collection (Lund and Khanna, 1989). Chosen frequencies are converted to discrete, noninteger values such that an integer number of cycles fits into the array, thus avoiding aliasing problems with the DFT. As a consequence, every frequency is a multiple of the fundamental sampling frequency 24.41 Hz. These programs were also run with a smaller step size of 25 microseconds. The Nyquist frequency is then 20 kHz and the frequency resolution of the DFT is 39.06 Hz. The use of a smaller step size illustrates the tradeoff between time and frequency resolution. Although the details of the waveforms at high signal frequencies sometimes changed with step size in our calculations, the qualitative nature of the results was independent of step size. The frequencies were always chosen such that the subharmonic frequency (the component at 1/2 the signal frequency) also fell into one of the discrete sampling bins of the computer operation and therefore could be observed.

The integration was always started with the initial conditions $x(0)=x'(0)=0$ to avoid the added complexity of studying the effects of perturbed initial conditions. No analysis of sensitivity to initial conditions was attempted because the focus of the present work is on the modeling of a biological system with a limited, but unknown, range of starting displacements and velocities. Since our current interest is on steady-state behavior, startup transients were removed by integrating for a number of steps before storing any solutions in the array. All of the results illustrated in the figures were constructed with a delay of 10,000 points, which is 0.400 seconds for a step size of 40 microseconds and 0.250 seconds for a 25 microsecond step size. The time course of the stored response was sufficiently long so that convergence to a limiting motion could usually be observed.

Results are shown in the form of displacement waveforms and their Fourier spectra, velocity waveforms and their spectra, phase-space projections, and plots of the velocity harmonics as a function of signal frequency. The spectra were obtained by a fast-Fourier transform (FFT) operation on the discrete array containing the sampled time waveform.

Both velocity and displacement are of interest in a complete dynamical study of a nonlinear system and both are needed to fully describe the state of the system at any give time. The displacement plotted against the velocity is the phase-space projection of the motion. It provides a useful representation of the complete information (state) of the dynamical system. By plotting points of displacement against velocity at successive times, a curve in phase space is traced out in which time is eliminated as an explicit variable. For example, the response of a linear oscillator gives rise to an elliptical phase-space projection. The phase-space projection is therefore useful in visualizing the deviations from an ellipse, which represent deviations of the motion from sinusoidal behavior.

Nonlinear oscillators can exhibit deterministic chaos, in which case the phase-space projection trace does not repeat itself and is never periodic. Its spectrum is then continuous. Such motion is not necessarily ergodic; although never repeating it remains confined to certain regions of the phase-space projection, a so-called strange attractor. A nonlinear system requires at least 3 (or 1.5 depending on nomenclature) degrees of freedom before there is a possibility for it to exhibit chaotic behavior. The bilinear oscillators have two degrees of freedom (displacement and velocity); however because they are nonautonomous (a forced system in which time is an explicit variable in the equation of motion), they have an extra degree of freedom that allows for the possibility of chaotic motion. Chaos does not necessarily exist for all possible starting positions of the oscillator nor for all

possible coefficient (parameter) values. For given coefficients, chaotic solutions can exist for certain starting values while periodic solution limit cycles, or simple attracting points, exist for others. Solutions are then said to coexist in the phase space. This topic is of current interest in the field of nonlinear dynamical systems (Thompson and Stewart, 1986; Berge, Pomeau and Christian, 1986).

RESULTS

Solutions for the sinusoidally forced bilinear resistance oscillator were obtained by using the values $A_o=100$ dynes, $m=1\times10^{-6}$ g, $r_1=0.001$ dyne-sec/cm, $r_2=0.003$ dyne-sec/cm, and $k=4$ dyne/cm in Eq. (1). The solutions presented here are representative and not peculiar to this choice of parameters. The best frequency (CF) of this oscillator is given approximately by $(1/2\pi)(k/m)^{1/2}=317$ Hz.

In Figures 1–4, results are shown in the form of (a) displacement waveforms, (b) displacement waveform Fourier spectra, (c) velocity waveforms, (d) velocity waveform Fourier spectra, and (e) phase-space projections. Figure 1 shows data at $f_s=73$ Hz, below the CF; Figure 2 shows data at $f_s=317$ Hz (at CF); Figures 3 and 4 show data above CF, at $f_s=610$ and 806 Hz, respectively. The finer time resolution of 25 microseconds was used for these higher signal frequencies.

Examining the displacement waveform at the four frequencies indicates that the deviation of the waveshape from sinusoidal is greatest below CF and decreases as the signal frequency increases. Consistent with this, the number of harmonic components present in the displacement spectra is greatest below CF and decreases as the signal frequency increases. The maximal excursions of the displacement waveform, on the other hand, appear to be constant below CF but begin to vary at CF. These low-frequency fluctuations increase with increasing signal frequency. Correspondingly, the numbers and magnitudes of the low-frequency spectral components of the displacement increase with increasing signal frequency.

Below CF, the deviations of the velocity waveforms from sinusoidal behavior are even more pronounced than those of the displacement waveforms. These deviations, which are maximal near the peaks of the waveforms, decrease as the signal frequency increases. The low-frequency fluctuations observed in the velocity waveform, on the other hand, are less pronounced than those in the displacement waveform since the velocity is the derivative of the displacement and therefore emphasizes high frequency spectral components. The velocity spectra follow the same trend as the displacement spectra with signal frequency.

The phase-space projections evidence nonelliptical and asymmetric behavior at all signal frequencies. Below CF, there are small deviations in the overlap of successive cycles. These deviations increase with increasing signal frequency and are a manifestation of the anharmonic components of the motion. The phase-space projection trace can be described as moving from one limit-cycle ellipse for positive displacement [and $r(x)=r_1$] to another ellipse of different size for negative displacement [and $r(x)=r_2$]. When the resistance values differ only slightly, the two ellipses are nearly the same and the transitions are relatively smooth. The velocity waveform exhibits a slight rectification at all frequencies.

The relative magnitudes of the first four velocity harmonics are shown as a function of signal frequency in Figure 5. These illustrate that the velocity tuning observed at the fundamental frequency is quite different from that observed at the second, third, and fourth harmonics. No subharmonic response is present. The frequencies of maximal response (best frequencies) of the second and third harmonics are lower than that of the fundamental. For this set of parameters, the low- and high-frequency responses of these curves have steeper slopes than that of the fundamental. The fourth harmonic displays a double peak and crosses the third-harmonic curve.

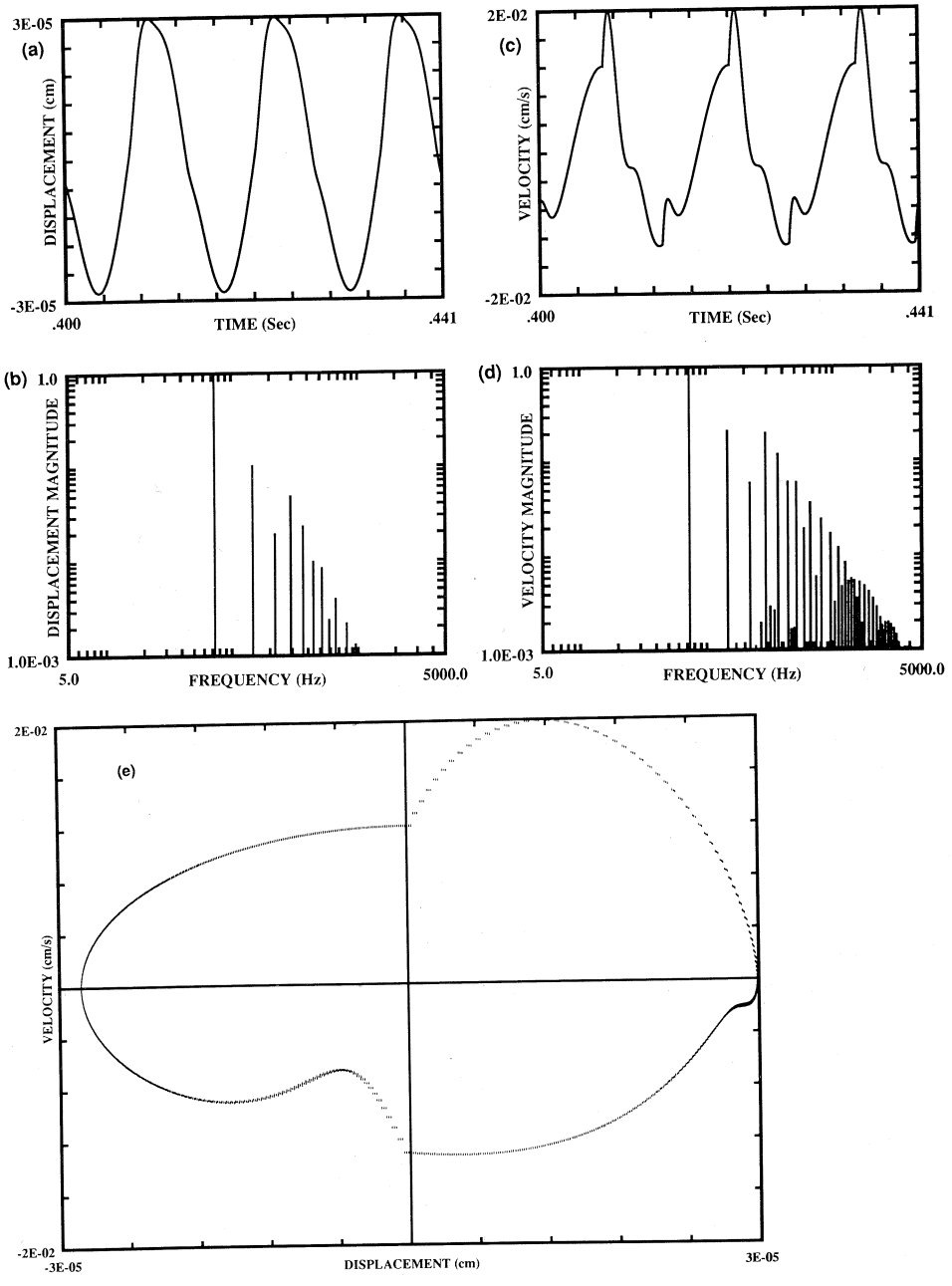

Fig. 1. Response of the bilinear resistance oscillator to a signal frequency f_s=73 Hz (below CF). (a) Time waveform of the displacement. The response is nonsinusoidal, particularly at its positive peaks. (b) Fourier spectrum of the displacement waveform. The large number of harmonics (9 are visible) confirms the nonsinusoidal nature of the waveform. The ratio of the displacement magnitude at dc (not shown) to the magnitude at the signal frequency is 0.001. (c) Time waveform of the velocity. The waveform peaks deviate most from sinusoidal behavior. (d) Fourier spectrum of the velocity waveform. The velocity, being the derivative of the displacement, exhibits a greater number of high-frequency components. (e) Phase-space projection. The trace is distinctly non-elliptical and asymmetric for both positive and negative displacements and velocities.

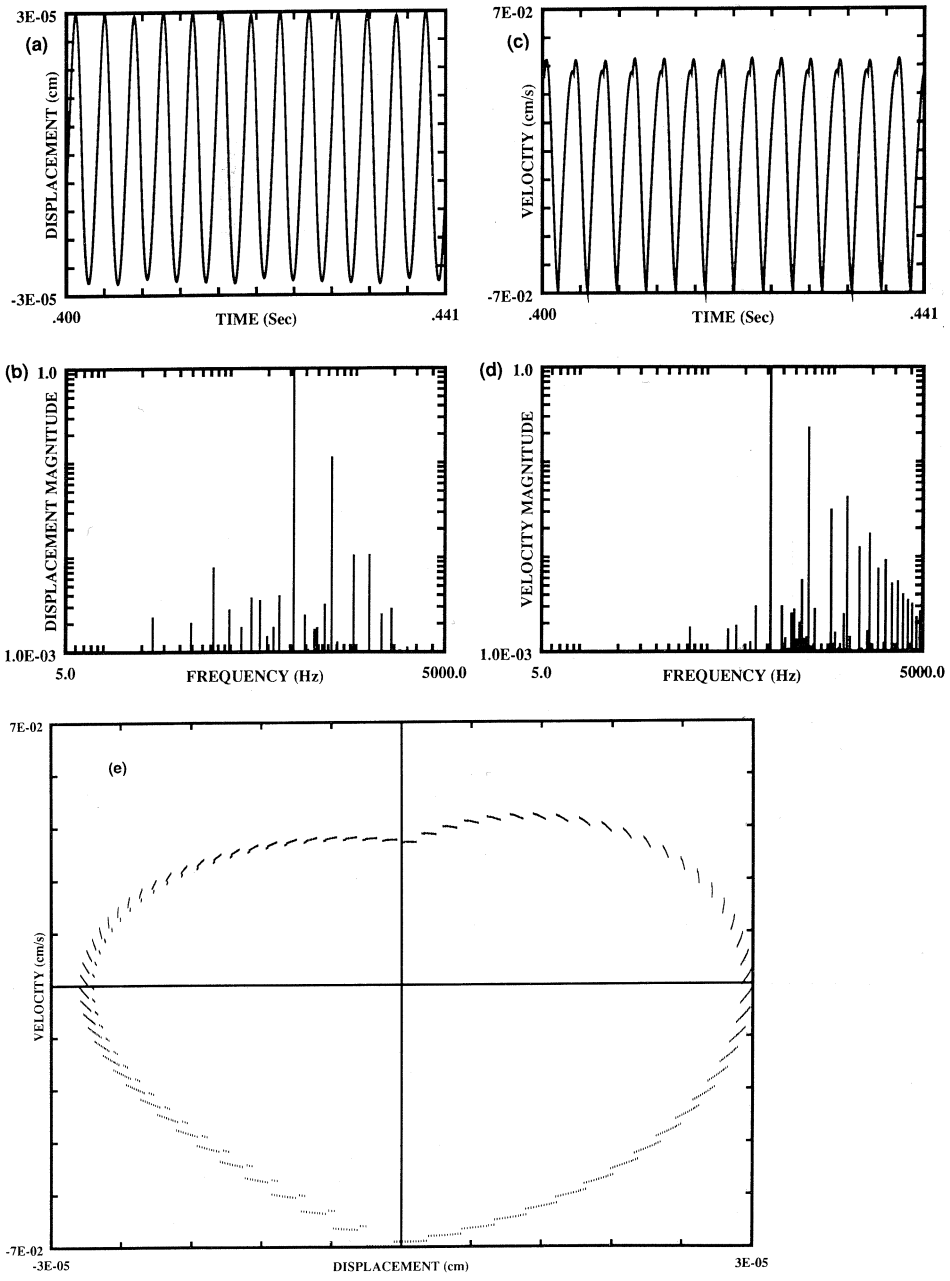

Fig. 2. Response of the bilinear resistance oscillator to a signal frequency f_s=317 Hz (at CF). (a) Time waveform of the displacement. The response appears to be quite sinusoidal. (b) Fourier spectrum of the displacement waveform. Although five harmonics are readily seen, only the second harmonic is comparable to the value seen at 73 Hz in Figure 1(b). Spectral components below 317 Hz are also visible. The ratio of the displacement magnitude at dc to the magnitude at the signal frequency is 0.02. (c) Time waveform of the velocity. Again, the waveform peaks deviate most from sinusoidal behavior. (d) Fourier spectrum of the velocity waveform. The number of high-frequency harmonics is greater than in the displacement spectrum. (e) Phase-space projection. The non-elliptical trace shows more symmetry for positive and negative displacements than for positive and negative velocities. The trace does not repeat itself on successive cycles; rather it slowly drifts back and forth as can be seen on the computer screen as it is being formed.

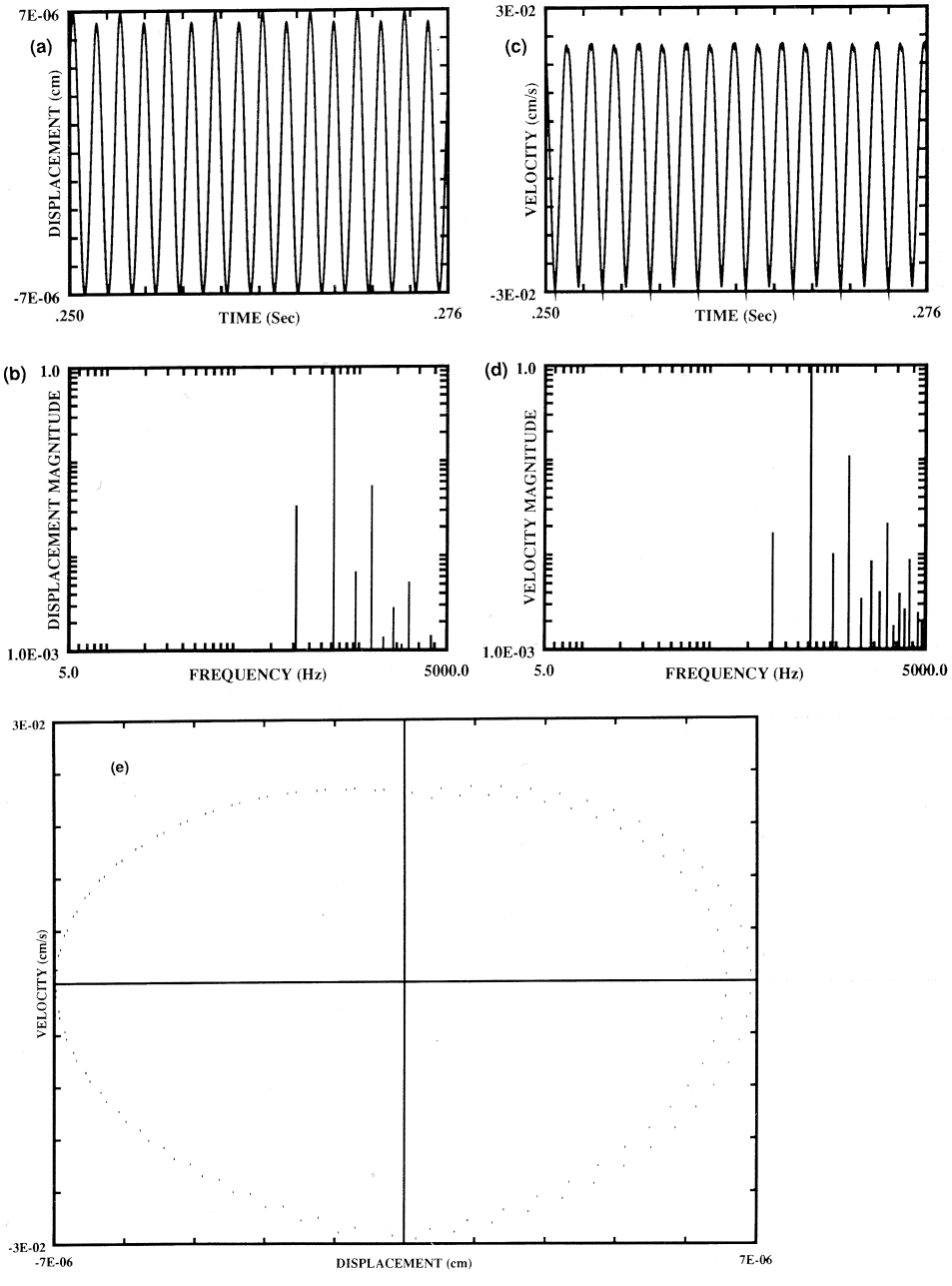

Fig. 3. Response of the bilinear resistance oscillator to a signal frequency f_s=610 Hz (above CF). (a) Time waveform of the displacement. The response has a sinusoidal character but successive cycles of the waveform clearly exhibit different heights. (b) Fourier spectrum of the displacement waveform. Only three harmonics are readily seen, but a strong spectral component appears below the signal frequency at about 300 Hz, which is near the CF of the oscillator. The ratio of the displacement magnitude at dc to the magnitude at the signal frequency is 0.07. (c) Time waveform of the velocity. Again, the waveform peaks deviate most from sinusoidal behavior. (d) Fourier spectrum of the velocity waveform. Five harmonics are visible. (e) Phase-space projection. The trace shows more pronounced amplitude deviations for positive displacements.

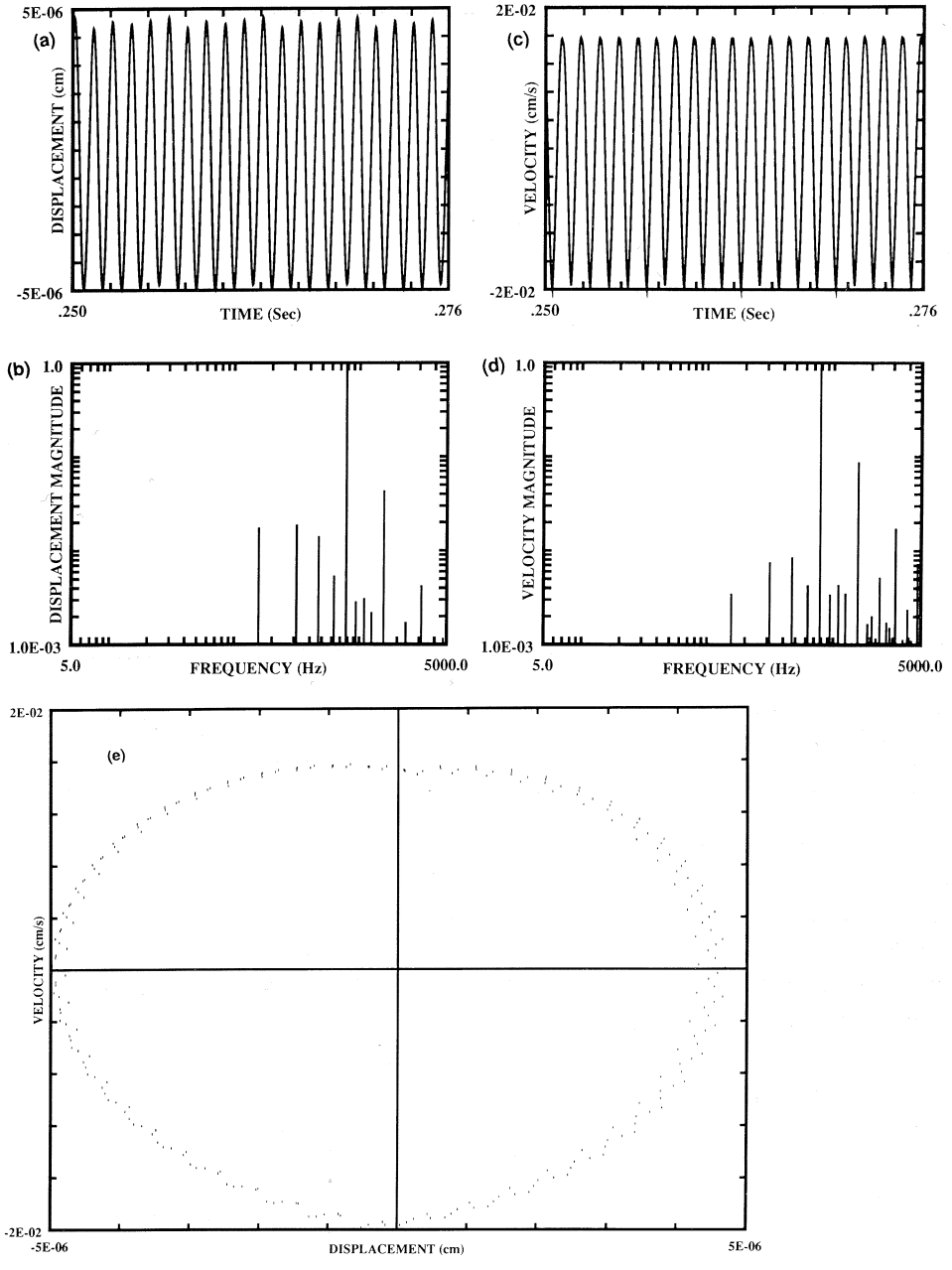

Fig. 4. Response of the bilinear resistance oscillator to a signal frequency f_s=806 Hz (well above CF). (a) Time waveform of the displacement. Nonrepetitive jumps in the heights of successive cycles are evident. (b) Fourier spectrum of the displacement waveform. Three harmonics are clearly visible as well as spectral components below the signal frequency. The ratio of the displacement magnitude at dc to the magnitude at the signal frequency is 0.10. (c) Time waveform of the velocity. Because the velocity is the derivative of the displacement, it deemphasizes the low-frequency jumps that are so clearly evident in the displacement waveform. (d) Fourier spectrum of the velocity waveform. Three harmonics can be seen. Note the deemphasis of the low-frequency spectral components. (e) Phase-space projection. The trace does not repeat itself and manifests slow fluctuations in all quadrants of the phase-space.

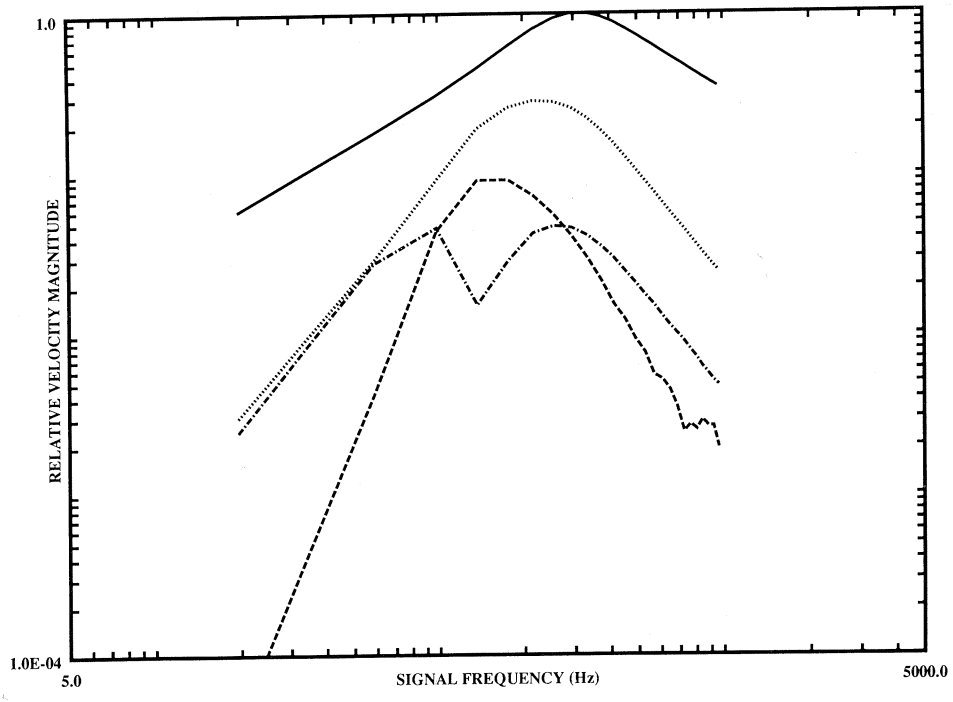

Fig. 5. Relative velocity-magnitude frequency-response curves for the bilinear resistance oscillator. The curves represent the magnitude of the first four velocity harmonics, plotted as a function of the applied signal frequency. The curves are coded as follows: fundamental (solid curve), 2nd harmonic (dotted curved), 3rd harmonic (dashed curve), 4th harmonic (dash-dot curve).

CONCLUSION

For the bilinear resistance oscillator model, the number and magnitude of the harmonic components in the displacement and velocity Fourier spectra are maximal at a signal frequency somewhat below CF and decrease with increasing signal frequency. Strong anharmonic components are present in the spectra at all signal frequencies.

ACKNOWLEDGEMENTS

This work was supported by the National Institutes of Health and the National Science Foundation. We are grateful to Evan Goldstein and David Lund for computer assistance.

REFERENCES

Berge P, Pomeau Y, Christian V (1986). Order within chaos. New York: Wiley & Sons.

Keilson SE, Teich MC, Khanna SM (1989). Models of nonlinear vibration. III. Oscillator with bilinear mass. Acta Otolaryngol (Stockh) Suppl 467: 257–264.

Lund DT, Khanna SM (1989). A digital system for the generation of acoustic stimuli and the analysis of cellular vibration data. Acta Otolaryngol (Stockh) Suppl 467: 77–89.

Press WH, Flannery BP, Teukolsky SA, Vetterling WT (1986). Numerical recipes. Cambridge: Cambridge Univ. Press: Chap. 15.

Scraton RE (1984). Basic numerical methods. London: Edward Arnold.

Teich MC, Keilson SE, Khanna SM (1989). Models of nonlinear vibration. II. Oscillator with bilinear stiffness. Acta Otolaryngol (Stockh) Suppl 467: 249–256.

Thompson JMT, Stewart HB (1986). Nonlinear dynamics and chaos. New York: Wiley & Sons.